Information Fusion 95 (2023) 199–214

Contents lists available at ScienceDirect

Information Fusion

journal homepage: www.elsevier.com/locate/inffus

Characteristic evaluation via multi-sensor information fusion strategy for spherical underwater robots

Chunying Li [a], Shuxiang Guo [a,b,*]

[a] Graduate School of Engineering, Kagawa University, Takamatsu. 761-0396, Japan
[b] Key Laboratory of Convergence Medical Engineering System and Healthcare Technology, Ministry of Industry and Information Technology, School of Life Science and Technology, Beijing Institute of Technology, Beijing, 100081, China

ARTICLE INFO

Keywords:
Multi-source information fusion (MSIF)
Attitude estimation
Positioning
Obstacle avoidance
Spherical underwater robots (SURs)
BPNN method

ABSTRACT

Currently, most of the existing fusion methods ignore the rich multi-source information of different types of sensor nodes in the underwater unknown environment, which makes it challenging for Autonomous Underwater Vehicles (AUVs) to accurately perceive the external environment and make actionable decisions. Considering the key issues such as attitude estimation, positioning and obstacle avoidance involved in performing AUV tasks, this paper proposed a Multi-Source Information Fusion (MSIF) model for Spherical Underwater Robots (SURs) we developed based on various low-cost sensors. Multi-source information from an Inertial Measurement Unit (IMU), Pressure Sensor Array (PSA), Obstacle Avoidance Sensor Array (OASA), Depth Sensor (DS), Looking-Down Camera (LDC) and Acoustic Communication System (ACS) were fused to enable SUR to obtain high-precision estimated data for attitude estimation, positioning and obstacle avoidance, etc. More precisely, according to the correlation between the sensors, the optimized model was constructed to compensate for angle errors, velocity errors, orientation errors, etc. Subsequently, a machine learning method using Back Propagation Neural Network (BPNN) was proposed to improve the accuracy and effectiveness of the MSIF model through feature selection, data training, and feature estimation, etc. Finally, a series of experiments were performed under different scenarios, such as motion and obstacle avoidance experiments. The theoretical derivation and comprehensive evaluations demonstrated the effectiveness and feasibility of the proposed model, which provided a new reference value for solving issues such as attitude estimation, positioning and obstacle avoidance of AUVs.

1. Introduction

In recent years, underwater robots have been increasingly used in underwater salvage, marine exploration, resource development, etc. [1–3]. Especially AUVs are gradually assisting or replacing humans to perform some dangerous and challenging tasks. Thus, improving the underwater work efficiency and capability of AUV's control system, such as navigation and positioning accuracy, fault tolerance, robustness, and anti-disturbance, is a hot topic.

AUVs employing a single sensor lack the ability to sense the external environment fully and reliably [4–5]. Thus, high autonomy and environmental perception are considerable for AUVs in uncertain underwater environments. MSIF technology is an effective way to improve the perception ability of the robotic system. By complementing, supporting, and correcting each other, more detailed information is provided for AUV, making its action behavior more accurate [6–7]. MSIF also enhances the control system's robustness and anti-disturbance performance from the perspective of information presentation. Furthermore, some issues in AUV attitude adjustment [8], localization [9], autonomous motion [10], etc., require comprehensive consideration of information quality, and MSIF is an important guarantee for improving the quality of data analysis and processing.

As mentioned above, this paper aims to combine data across multiple sensor nodes to draw more accurate and specific inferences than a single sensor [11–13]. MSIF now mainly focuses on the application of land-based intelligent robots, while related research on AUVs is relatively scarce. This work is based on the SUR prototype we proposed [1, 4-5,14], and uses MSIF technology to enhance SUR's environmental perception and execution capabilities, so that SUR can interact with the external environment to adapt to the complex and unknown underwater environment. In addition, SUR motion control and decision-making can be improved by processing the collected information.

* Corresponding author.
E-mail address: guo.shuxiang@kagawa-u.ac.jp (S. Guo).

https://doi.org/10.1016/j.inffus.2023.02.024
Received 14 October 2022; Received in revised form 14 February 2023; Accepted 16 February 2023
Available online 21 February 2023

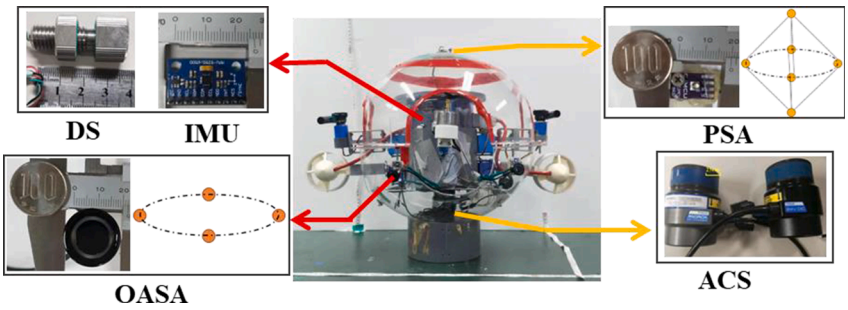

Fig. 1. The sensor system carried of the SUR.

Here, we further conclude some research related to MSIF. *Yager* [15] pointed out the importance of MSIF and the issues that need to be considered. *Zhang* et al. [16] mentioned that the model construction and fusion of MSIF for different scenarios is the core problem to be solved urgently. *Liu* et al. [17] proposed an online Remaining Useful Life (RUL) prediction mechanism for machining tools using MSIF technology, aiming to estimate unpredictable failures and unscheduled maintenance to improve equipment reliability. *Che* et al. [18] employed evidence theory, probability theory, and information entropy to deal with the information fusion of uncertain data in a Multi-Source Information System (MSIS), which created a novel route for granular computing. In addition, the application of MSIF on Unmanned Aerial Vehicles (UAV) has been increasing [19–21]. *Nguyen* et al. [22] developed a fusion measurement strategy based on multi-sensors, such as vision sensors, Inertial Measurement Unit (IMU), ranging sensors, lidar odometry subsystems, etc., which provides a reliable, accurate, and flexible scheme for UAV applications in the real world. *Liu* et al. [23] designed a multi-target collaborative navigation system using the MSIF method, aiming to improve the efficiency and accuracy of multi-UAV localization. For some underwater application scenarios, such as undersea tunnel construction, *Zhou* et al. [24] proposed a new risk assessment method by integrating jobsite monitoring data, design data, environmental data, etc., and the proposed system assessed from multiple dimensions to avoid accidents. *Lighthill* [25] used the lateral-line sensors to significantly increase the resistance for a regularly swimming clupeid fish's motion. Most of the above-mentioned MSIF technologies are mainly studied for data training or UAV applications, while the MSIF for AUV is relatively lacking. In addition, MSIF is of great significance in various issues underwater, such as localization and attitude estimation, but how to utilize the characteristics of multi-sensor nodes still faces huge challenges.

In our previous research, we have made some progress in the control system for SUR [26–30]. In [5], an obstacle avoidance model based on multi-ultrasonic sensor array is proposed considering SUR kinematic and dynamic models. In [14], an attitude regulator is designed based on the counterweight mechanism, and the Back-stepping Sliding Mode Control (BSMC) method is implemented considering the uncertainty and nonlinearity of the SUR model. In [6], some simulations are conducted using Gazebo simulator on the self-localization system with multi-sensor. In addition, some positioning methods are studied such as Simultaneous Localization and Mapping (SLAM), Proportional Integral Derivative (PID) [28] and Generalized Prediction Control (GPC) [29]. And some obstacle avoidance methods are studied such as Fuzzy Control (FC) [28] and Ant Colony Optimization (ACO) [30]. However, we found that with the increasing underwater mission requirements, increasingly sensors are installed, while fusing the information collected by multiple sensors effectively is challenging.

In this study, an MSIF model is proposed to effectively fuse multiple data and establish the correlation between sensor nodes. The contributions of this paper are summarized in the following three aspects:

1) Firstly, compared with our previous works, a comprehensive set of sensors, i.e. DS, PSA, OASA, IMU, LDC and ACS, are fused. To integrate such a comprehensive sensor set, a more general MSIF scheme is developed to improve the practical application value of SUR in performing tasks. The proposed MSIF model improves the accuracy of motion recognition parameters. Moreover, the relationship between multiple sensors is established and optimized, which can comprehensively evaluate the performance of the SUR, reflecting the tight coupling and fusion between multiple data.
2) Secondly, traditional methods generally only consider the design or measurement of individual data sources, and lack constructing the observation model for MSIF. In this work, our method considers multi-sensor information, such as distance, position, orientation, and motion perception, which reduces errors in positional offset, velocity, and tracking.
3) Finally, the link between sensor nodes is established through the optimized prediction model, which ensures the robustness, anti-disturbance and effectiveness of the SUR control system. Then, a series of experiments are performed to verify the performance of the proposed MSIF model.

The remainder of this paper is organized as follows: Section 2 describes the system overview of SUR and the MSIF model proposed in this paper. Then, the optimized prediction model for SUR is developed in Section 3, including the attitude estimation model, velocity estimation model, depth estimation model, obstacle avoidance model and multi-sensor optimal estimation model. Afterward, Section 4 carries out a series of experiments in real environments, such as motion and obstacle avoidance experiments. Finally, in Section 5, we further comprehensively analyze and discuss the performance of the proposed MSIF model. Finally, Section 6 concludes the paper.

2. System and methods for the SUR

In this section, the overall system of the SUR is first introduced. Then the idea of multi-sensor fusion is described, including IMU, PSA, OASA, DS, LDC and ACS. Next, we introduce the machine learning tools applied to the MSIF model.

2.1. SUR system overview

SUR is a miniature AUV inspired by jellyfish for underwater missions [1,4,9,31-32]. Its size and total weight are about 54 cm and 7.9 Kg, respectively. It mainly consists of two 3-D printed half shells, the power supply unit, the driving unit, the processing system, and the sensor unit. The SUR has a hybrid propulsion device [31–32] (multi-water-jet thrusters and propellers) that enables multi-mode switching, which allows the SUR to select the motion mode from the starting position to the target according to the actual environmental conditions [4], improving execution efficiency and shortening operation time. Furthermore, in unknown underwater environment, the SUR perceives and reflects the surrounding environment information mainly through the carried

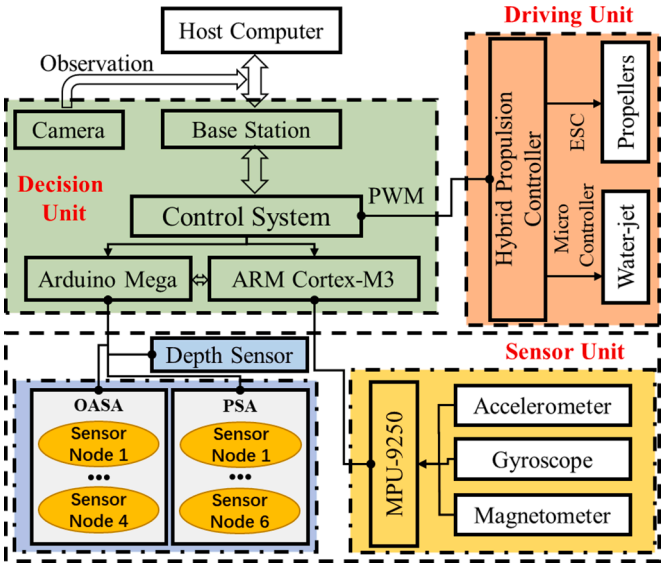

Fig. 2. Diagrammatic sketch of the control system of the SUR.

sensor unit, mentioned in [1,5,30,33]. This work aims to process data from the sensor unit based on different features to obtain a fusion model.

The sensor unit of SUR used during the experiments mainly consists of a micro data modem ACS [34], DS MS5837–30BA, PSA which is composed of six CJMCU-5837 pressure sensors, OASA which is composed of four JSN-SR0T4 ultrasonic sensors, IMU MPU-9250, see Fig. 1. The CJMCU-5837 sensor has a new generation with a resolution of 2 mm with size (length x width) of 18 mm x 10 mm. For the PSA, one on the top, one on the bottom and four on the center track. The JSN-SR0T4 ultrasonic sensor can provide a 20–600 cm non-contact distance sensing function, ranging in accuracy up to 2 mm (with a diameter 12 mm). And the OASA is located in the center track. The distribution of the sensor array depends on the robot's motion features and hydrodynamic environment. Then, information from all sensors is transmitted to the processing unit, consisting of Arduino Mega 2560 and ARM Cortex-M3, for sensor fusion and state estimation etc. [33–35].

Fig. 2 shows the schematic diagram of the SUR control system. In the driving unit, the actuator uses a hybrid propulsion device that uses water-jet thrusters to achieve low-velocity stable motion during turns, and use propeller or hybrid propulsion to achieve fast-flexible motion when there are moving obstacles or in unrestricted space, etc. [4]. In addition, the attitude and heading of the SUR are mainly controlled by the IMU MPU9250, which consists of a three-axis accelerometer, a three-axis gyroscope, and a three-axis magnetometer. The yaw, pitch, roll, angular velocity, and angular velocity variables of the SUR are output in the control system with ARM Cortex-M3 at a sampling rate of 50 Hz. Arduino Mega control board for PSA and OASA data acquisition and pre-processing. The PSA is mainly used to measure the static pressure of the SUR under water, which can be used for attitude estimation and depth estimation, detailed in Section 3. When the SUR is moving underwater, the observation system, which is composed of the host computer system, base station and an LDC, is used to realize the SUR positioning. Noted that the transmission rate of the ACS and the host computer is 50 Hz.

2.2. Data fusion description

Based on the control system mentioned above, we know that the SUR is equipped with multiple sensors. Thus, to comprehensively evaluate the performance (such as effectiveness, accuracy, robustness and anti-disturbance, feasibility) and test results of the SUR when performing tasks underwater, an MSIF model combined with the BPNN method is proposed as part of the SUR skill assessment. Metric evaluation system

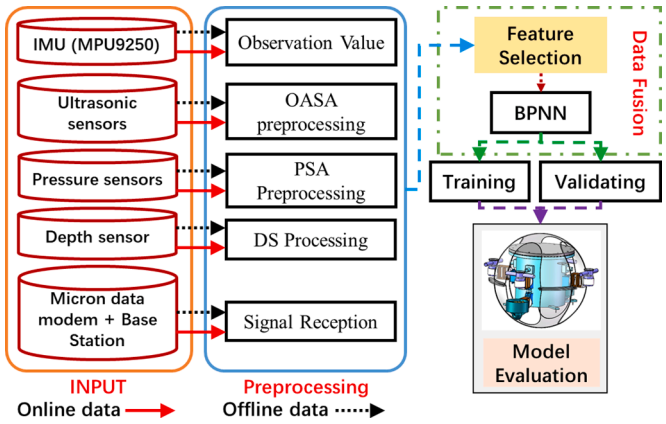

Fig. 3. The evaluation system workflow for SUR based on the MSIF model.

workflow is presented in Fig. 3, including the data preparation, pre-processing, data fusion and model evaluation.

Here, we first describe the role of various sensors. For the IMU, as the most critical sensor in positioning and attitude estimation, it can be used for basic physical quantities such as measurement, acceleration and rotation velocities. For the PSA, it can be used for external environment perception, motion recognition and velocity measurement. For the OASA, it can be used to detect the distance of surrounding obstacles in real-time so that the SUR can safely perform tasks by avoiding obstacles. As can be seen that a certain relationship can be established between these sensor data, such as velocity and position, etc. The real-time correction between the data can reduce the overall error, correct the positional drift of the SUR in all directions, and can greatly adjust the robot's attitude and velocities, real-time obstacle avoidance, etc. Thus, this paper designs the following IMU/OASA/PSA/DS data fusion model. In this way, when a certain sensor signal fails, the absolute position error can be calculated through other sensor data through communication and observation. It aims to solve the problems such as fusion model construction, data processing, factor derivation, etc., and enhance the predictive accuracy of predictive mode by combining different data sources.

Multi-source data should be pre-processed before fusion [36–37]. First, due to the influence of unavoidable factors such as the external environment, the data collected by multi-sensors have a lot of redundant information, which will interfere with signal analysis to a certain extent. There is therefore a need to filter out poorly measured values and perform signal pre-processing. The filtering of these poorly measured values is mainly limited by a defined threshold, and only those within the threshold are passed on. Then, for the IMU data, after transforming coordinates from t_n to t_{n+1}, the PSA values are combined to adjust the robot's attitude. For the OASA data, the adjustment of robot motion is mainly combined with the DS data. Finally, all measurements at a certain time $[t_n, t_{n+1}]$, including the interpolated values, are used in the design of the optimized model by constructing cost factors to estimate the state estimation and attitude prediction.

2.3. Application method of BPNN based on MSIF

BPNN, as a commonly used supervised machine learning tool, has a wide range of applications in many fields such as optimization, signal processing, prediction, perception, intelligent control and fault diagnosis [38–40]. While on a mission, the SUR receives and stores multi-sensor signals. The prediction system mainly involves two types of data, offline and online, as shown in Fig. 3.

For offline signal data processing, the purpose is to classify the data, correct the deviation and judge the execution action. After pre-processing, the relevant features are extracted by denoising the time domain and frequency domain features. Optimal features related to the SUR parameter and behavior are selected and classified. These selected

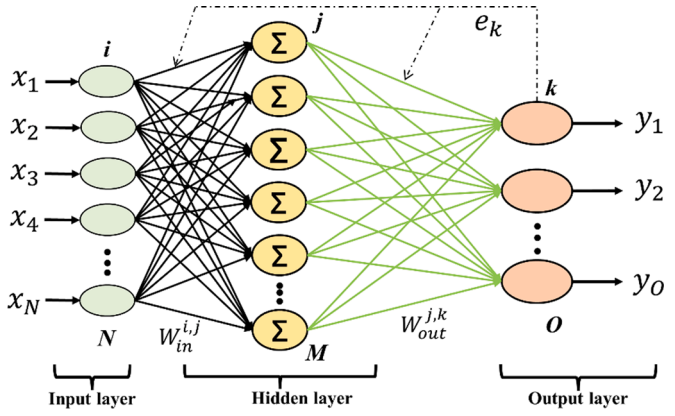

Fig. 4. The structure of the BPNN model.

features are trained using the BPNN method to predict and improve the SUR accuracy and efficiency. Simultaneously, online signal data processing is triggered when BPNN model training and validation are completed. After completing the feature extraction and selection, the optimized features will be transferred to the MSIF model, which will be compared and controlled in conjunction with the result of BPNN.

The structure of BPNN consists of input layer *X(N)*, hidden layer *H (M)* and output layer *Y(O)*, [41] as shown in Fig. 4. Where $i \in \{1, 2, \ldots, N\}, j \in \{1, 2, \ldots, M\}, k \in \{1, 2, \ldots, O\}$ is the number of per layer neurons. t_k and e_k express the desired output value and error, respectively. In addition, it also can arbitrarily fit multi-dimensional data problems. The input and output layers can be represented as:

$$\begin{cases} X(N) = [x_1, x_2, \ldots, x_N] \\ Y(O) = [y_1, y_2, \ldots, y_O] \end{cases} \tag{1}$$

The input expression of the hidden and output layers can be expressed, respectively, as follows:

$$\begin{aligned} I_{Hj} &= \sum_{i=1}^{N} W_{in}^{i,j} x_i - b_j \\ I_{Ok} &= \sum_{j=1}^{M} W_{out}^{j,k} O_{Hj} - b_k \end{aligned} \tag{2}$$

where I_{Hj} and I_{Ok} represent the input of the neuron of hidden layer j and output layer k respectively. b_j and b_k denote the corresponding threshold of the neuron j and k, respectively.

The output expression of the hidden and output layers can be expressed, respectively, as follows:

$$\begin{aligned} O_{Hj} &= f_H(I_{Hj}) = f_H\left(\sum_{i=1}^{N} W_{in}^{i,j} x_i - b_j\right) \\ O_{Ok} &= f_O(I_{Ok}) = f_O\left(\sum_{j=1}^{M} W_{out}^{j,k} * O_{Hj} - b_k\right) \end{aligned} \tag{3}$$

where O_{Hj} and O_{Ok} represent the output of the neuron of hidden layer j and output layer k respectively.

To perform the mission appropriately, the output error is calculated as follows:

$$e_k = t_k - y_k \tag{4}$$

In the layer-by-layer transmission of the signal, the weight and threshold are continuously adjusted by the error e_k to make the output value closer to the desired value. In this study, the Root Mean Squared Error (RMSE) is used to represent the prediction error of the output layer, as

$$RMSE = \sqrt{\frac{1}{n}\sum_{k=1}^{O}(t_k - y_k)^2} \tag{5}$$

Table 1
Specific parameters of the machine learning tools.

Parameters	SVM	NB	RF	LR	BPNN
Network layers	3	3	3	3	**3**
Network structure	3	0.04	20	0.3	**6 × 14 × 1**
Training function	svmtrain	fitcnb	treebaggar	sigmoid	**sigmoid**
Total dataset size	12,000	12,000	12,000	12,000	**12,000**
Learning rate	0.1	0.1	0.1	0.1	**0.08**

In addition, datasets in various locomotion experiments are used for training, including linear motion, diving motion, rising motion, comprehensive motion, and obstacle avoidance motion. The dataset settings in motion experiments are as follows: 60% of the datasets are used for training, and 40% for testing. The input is the information of different types of sensor nodes, and the output is the optimized sensor information model. Then, BPNN is compared with some other machine learning tools, such as Logistic Regression (LR), Support Vector Machine (SVM), Naive Bayesian (NB) and Random Forest algorithm (RF) to verify its effectiveness.

For BPNN, the training function adopted the *train-Berger-Marquardt backpropagation method*, and the transfer function used the *sigmoid function*, as shown in Table 1. Noted that the number of nodes in the hidden layer is determined by the number of nodes *N* in the input layer according to *Kolmogorov's superposition theorem*, which satisfies 2*N*+2. For LR, the cost function was set to 0.3, and the learning rate was 0.1. For RF, the number of trees was 20 and the *treebaggar function* was used. For NB, the criterion value was set to 0.04 and the *fitcnb function* was used. For SVM, the *ploy-nominal kernel* and *svmtrain function* was chosen in training, and the value of *ploy-nominal* defaults to 3. The training results using five learning methods are presented in Section 5.3.

3. Establishment of the optimized prediction model

In this part, the optimized prediction model for the SUR is built in detail. Furthermore, some practical application problems, such as attitude estimation, velocity estimation, depth estimation and obstacle avoidance are solved. The correlation between multiple sensor nodes is established according to the sensor's physical characteristics, as shown in Fig. 5.

3.1. Attitude estimation model

In [42], it is mentioned that in real conditions the disturbances induced by the dynamic environment are not limited to a single dimension. The displacement deviation of SUR due to the lack of counterweight mechanism is mainly caused by pitch and roll angle changes [14]. To effectively compensate for these disturbances, we propose a novel attitude estimation model for SUR based on PSA and IMU.

For IMU, the roll and pitch angles can be solved by the accelerometer, and the yaw angle can be solved by the magnetometer. The rotation matrix R_E^B from the Earth coordinate frame *{E}* to the Body coordinate frame *{B}* is expressed as:

$$\begin{aligned} R_E^B &= R(-\phi, -\theta, -\psi) \\ &= \begin{bmatrix} c\theta c\psi & c\theta s\psi & -s\theta \\ -c\phi s\psi + s\phi s\theta c\psi & c\phi c\psi + s\phi s\theta s\psi & s\phi c\theta \\ s\phi s\psi + c\phi s\theta c\psi & -s\phi c\psi + c\phi s\theta s\psi & c\phi c\theta \end{bmatrix} \end{aligned} \tag{6}$$

where s and c represent sin and cos, respectively.

Assuming that the acceleration of the accelerometer is consistent with the acceleration of gravity, satisfies $a = g = (0, 0, 1)^T$. The accelerometer data is obtained through the rotation matrix R_E^B, yields,

$$a = R_E^B * g \tag{7}$$

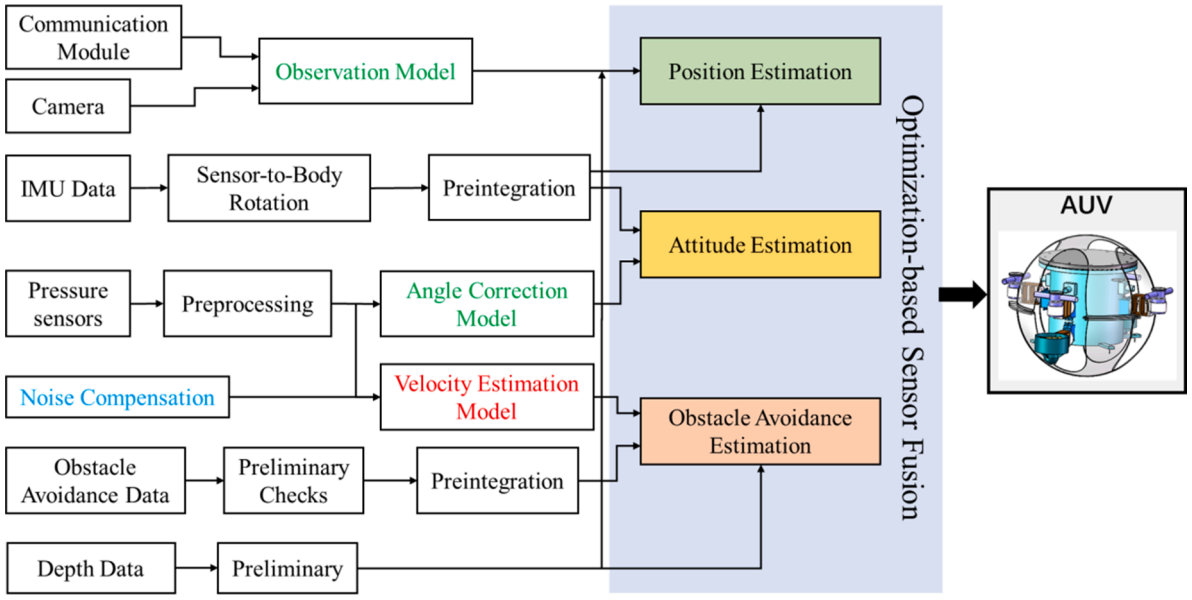

Fig. 5. Establishment of multi-sensor correlation and proposition of estimation model for the SUR.

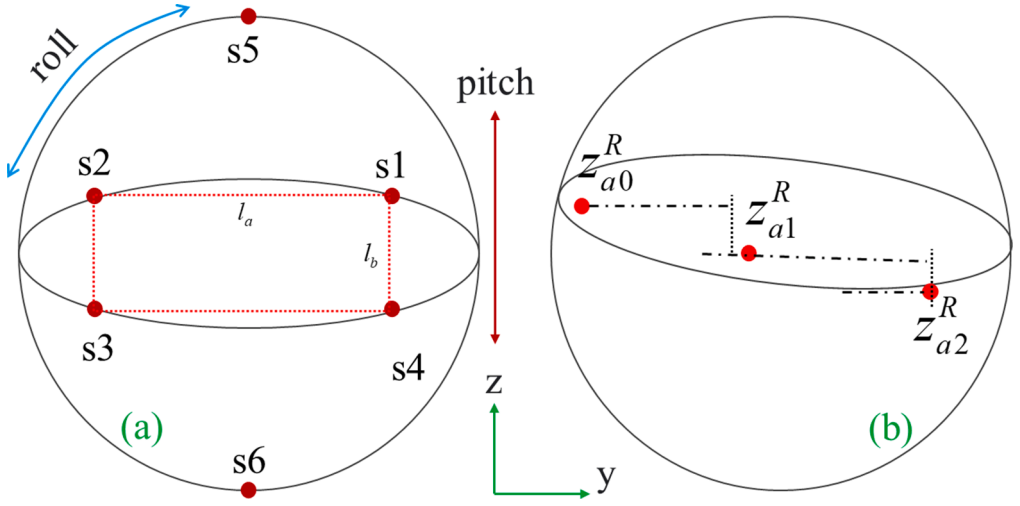

Fig. 6. Schematic of (a) attitude estimation using PSA, (b) The z-axis component of the pressure sensor for depth estimation.

where g is the acceleration of gravity.

The measured value a of the roll and pitch angles can be calculated, satisfies,

$$\begin{aligned} a &= [a_x, a_y, a_z]^T \\ &= [-s\theta, s\phi c\theta, c\phi c\theta]^T \end{aligned} \tag{8}$$

Thus, the roll and pitch angles can be expressed as

$$\begin{aligned} \phi &= \arcsin(a_x) \\ \theta &= -\arctan\left(\frac{a_y}{a_z}\right) \end{aligned} \tag{9}$$

Here, we use r_i to define the pressure measurement point relative to the frame $\{B\}$, which satisfies the Cartesian coordinate frame. The new coordinates related to roll and pitch angles satisfy:

$$r_i^R = r_i * R(\phi, \theta) \tag{10}$$

where $R(\phi, \theta)$ yields:

$$R(\phi, \theta) = \begin{bmatrix} c\theta & c\theta & -s\theta \\ s\phi s\theta & c\phi & s\phi c\theta \\ c\phi s\theta & -s\phi & c\phi c\theta \end{bmatrix} \tag{11}$$

As we mentioned, PSA can be used for attitude estimation, depth estimation (described in Section 3.3), as shown in Fig. 6. In this part, the PSA is used to compensate for the attitude.

The hydrostatic pressure component between the measurement points is calculated to correct the pressure difference, as shown in Fig. 6 (a). The difference between sensor *s1* and other sensors can be expressed as:

$$\begin{aligned} D_{s1s2} &= l_a \sin\phi \\ D_{s1s3} &= l_b \cos\phi \sin\theta + l_a \sin\phi \\ D_{s1s4} &= l_b \cos\phi \sin\theta \end{aligned} \tag{12}$$

Here we estimate ϕ and θ as state variables, then the observation side matrix can be expressed as:

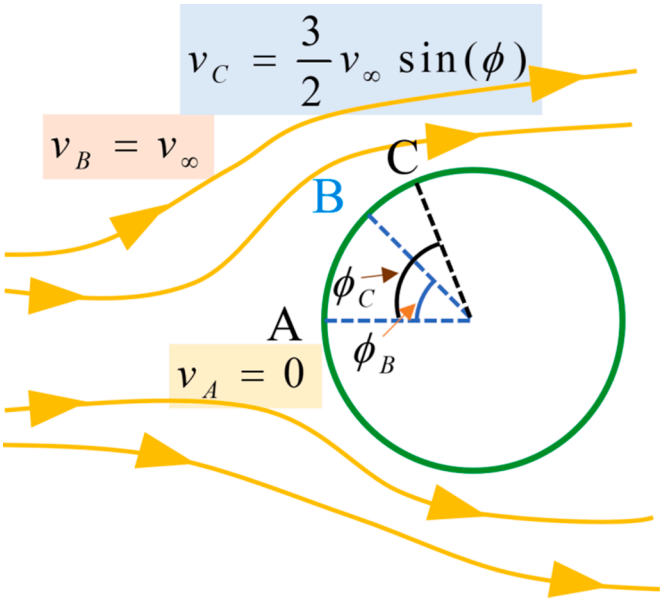

Fig. 7. The hydrodynamic on the surface of SUR body. The stagnation point on the SUR body is indicated by A, and the static point and arbitrary point are indicated by B and C, respectively.

$$E_{observe} = \begin{bmatrix} \frac{\partial D_{s1s2}}{\partial \phi} & \frac{\partial D_{s1s2}}{\partial \theta} \\ \frac{\partial D_{s1s3}}{\partial \phi} & \frac{\partial D_{s1s3}}{\partial \theta} \\ \frac{\partial D_{s1s4}}{\partial \phi} & \frac{\partial D_{s1s4}}{\partial \theta} \end{bmatrix} = \begin{bmatrix} 0 & l_a \sin\phi \\ l_b \cos\phi cos\theta & l_a \cos\phi - l_b \sin\phi \sin\theta \\ l_b \cos\phi \cos\theta & -l_b \sin\phi \sin\theta \end{bmatrix} \tag{13}$$

3.2. Velocity estimation model

Fig. 7 shows the hydrodynamic on the surface of SUR body which can be approximated by *Bernoulli's law* [43–44] based on incompressible flow and neglecting the elevation effect, the relationship between pressure p and velocity v_∞ at point B satisfies:

$$v_\infty = \sqrt{\frac{2(p_A - p_B)}{\rho}} = \sqrt{\frac{2\Delta p_{AB}}{\rho}} \tag{14}$$

where ρ represents the density of the water.

Assuming that the measurement point B is a stationary point on the SUR body, the relationship between the velocity at any position C and the free flow velocity can be described as:

$$v_c = \frac{3}{2} v_\infty \sin\phi_c \tag{15}$$

where ϕ_c is the angle between stagnation point A and measurement point C. Substituting Eq. (15) into (14) gives

$$v_\infty = \sqrt{\frac{2}{\rho} \frac{4\Delta p_{AB}}{9\sin^2\phi_c}} \tag{16}$$

Then the differential pressure component in the *z-axis* direction between the stagnation point A and the two additional measurement points C and C* can be corrected as

$$\begin{aligned} \Delta p_{c1} &= \Delta p_1 - (z^R_{a1} - z^R_{a0})\rho g \\ \Delta p_{c2} &= \Delta p_2 - (z^R_{a2} - z^R_{a0})\rho g \end{aligned} \tag{17}$$

According to the quadratic average of the pressure differences, we can drive that

$$\sqrt{\frac{\Delta p_{c1}^2 + \Delta p_{c2}^2}{2}} = \sqrt{\frac{\left(\frac{1}{2}\rho\left(\frac{3}{2}v_\infty \sin\phi_{c1}\right)^2\right)^2 + \left(\frac{1}{2}\rho\left(\frac{3}{2}v_\infty \sin\phi_{c2}\right)^2\right)^2}{2}} \tag{18}$$

To sum up, the compensated equation can be obtained as follow:

$$v_\infty = \sqrt[4]{\frac{2}{\rho^2}\left(\frac{4\Delta p_{AB}}{9\sin^2\phi_c}\right)^2 (\Delta p_{c1}^2 + \Delta p_{c2}^2)} \tag{19}$$

3.3. Depth estimation model

For the depth variation $\Delta h = \sqrt{\Delta h_{ps}^2 + \Delta h_{ds}^2}$ and velocity variation $\Delta v = \sqrt{\Delta v_{ps}^2 + \Delta v_{ds}^2}$ in the depth direction, they are calculated by the quadratic average of the PSA and DS sources.

To build the depth estimation model, firstly, the pressure difference between pressure sensors is derived using PSA.

Assume the pressure difference between the sensors consists of the vector Δp. If the sensor has n points, the vector Δp has *n-1* pressure differences as follows:

$$\Delta p = (\Delta p_1, \Delta p_2, \cdots, \Delta p_{n-1}) \tag{20}$$

As shown in Fig. 6(b), take Δp_1 as an example, the depth variation Δz_{h1} satisfies:

$$\Delta z_{h1} = z^R_{a1} - z^R_{a0} \tag{21}$$

where z^R_{a0}, z^R_{a1} represent the *z-axis* components between two adjacent measurement points.

Then, the pressure difference Δp_1 between p_2 and $\bar{p}_1$ satisfies $\Delta p_1 = p_2 - \bar{p}_1$. The depth variation of the pressure variable model in the depth direction can be calculated by:

$$\Delta h_{ps} = \frac{\Delta P_{ps}}{\rho g} \tag{22}$$

where ΔP_{ps} is the change in the mean value of the pressure data of the SUR from the initial time to time t.

The velocity in the depth direction varies as follows:

$$v_{ps} = \frac{\Delta h_{ps}}{t} \tag{23}$$

3.4. Obstacle avoidance model for SUR

In this paper, the velocity potential is related to the component of the translational velocity (*U, V, W*) based on the frame *{B}* and can be expressed as:

$$\Phi = U\Phi_U(X, Y, Z) + V\Phi_V(X, Y, Z) + W\Phi_W(X, Y, Z) \tag{24}$$

where *(X,Y,Z)* represents positions on the surface of the SUR in the body-fixed coordinate system. $\frac{dX}{dt} = U$, $\frac{dY}{dt} = V$, $\frac{dZ}{dt} = W$. Φ_U, Φ_V, Φ_W, respectively, represent the velocity potential alone the *OX-axis, OY-axis* and *OZ-axis* in frame *{B}*.

If $\delta = (\delta_X, \delta_Y, \delta_Z)$ is the position error of the target, then:

$$X = x + \delta_X, Y = y + \delta_Y, Z = z + \delta_Z \tag{25}$$

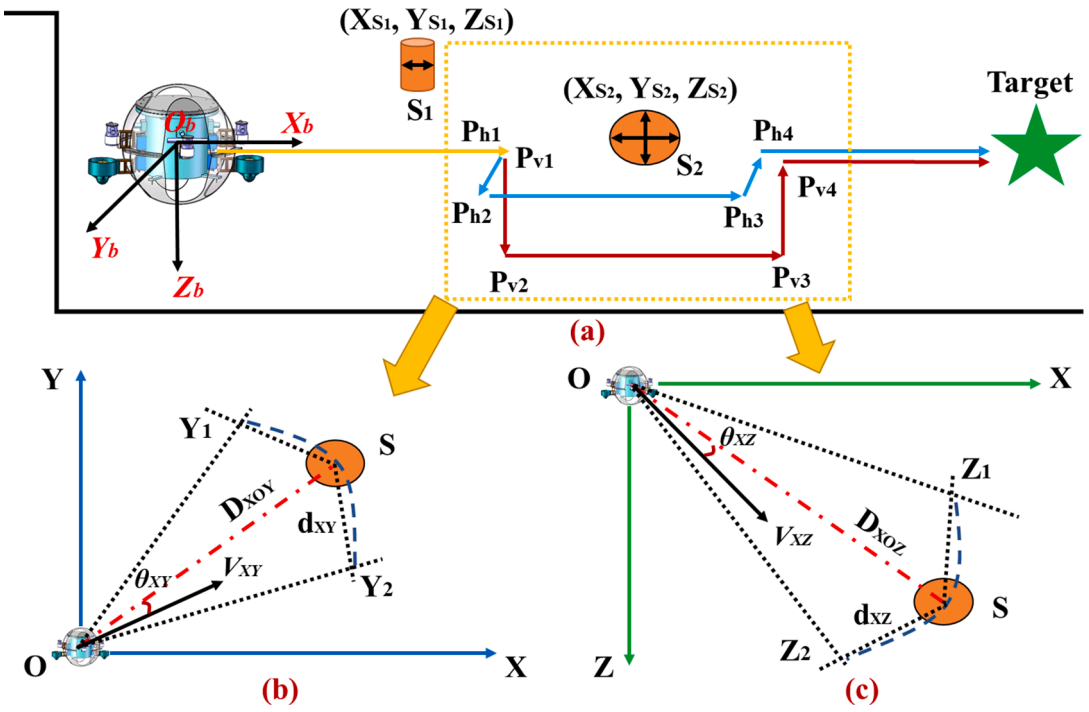

Fig. 8. SUR underwater obstacle avoidance decomposition diagram, (a) Relationship between SUR and obstacles (b) Horizontal motion (b) Vertical motion.

The distance d between the SUR and the target using the Taylor equation can be expressed as:

$$d = \rho_0 + \frac{x - x_0}{\rho_0}\delta_x + \frac{y - y_0}{\rho_0}\delta_y + \frac{z - z_0}{\rho_0}\delta_z \tag{26}$$

where ρ_0 is the initial state and (x,y,z) is the coordinate of the target. $(x-x_0)/\rho_0, (y-y_0)/\rho_0, (z-z_0)/\rho_0$ are the cosine value of x, y, z coordinate axes.

However, in underwater collision avoidance, puffing the obstacles (collision hazard area) conduces to improve the safety of execution and reach the target position successfully, as shown in Fig. 8. It can be seen that the SUR can avoid obstacles using horizontal motion and vertical motion, detailed in [4]. Considering the particularity of the SUR working environment, we divide the hazard area by establishing the corresponding three-dimensional velocity potential field, namely the horizontal plane collision area (as shown in Fig. 8(b)) and the vertical plane collision area (as shown in Fig. 8(c)).

It can be seen from Fig. 8(b) that the horizontal hazard area is OY_1SY_2, and V_{XY} is the relative velocity within this area. Similarly, in Fig. 8(c) the vertical hazard area is OZ_1SZ_2, and V_{XZ} is the relative velocity within this area.

If we assume that the velocity potential U is synthesized from the horizontal velocity potential U_H and the vertical velocity potential U_V, yields:

$$U = U_H \oplus U_V \tag{27}$$

where $\oplus$ represents the composite operator.

The horizontal velocity potential U_H represents the collision risk of the SUR in the horizontal plane, can be expressed as:

$$U_H = \begin{cases} U_{HD} \bullet U_{Ht} & if\,\theta_{xy} < \theta_H \\ 0 & else \end{cases} \tag{28}$$

where

$$\begin{aligned} \sin\theta_H &= \frac{d_{XY}}{D_{XOY}} \\ U_{HD} &= \frac{1}{D_{XOY}} \bullet \left(\frac{1}{|\sin\theta_{XY}|} - \frac{1}{\sin\theta_H}\right) \\ U_{Ht} &= \exp\left(-\frac{D_{XOY}}{|V_{XY}|\cos\theta_{XY}}\right) \end{aligned} \tag{29}$$

where θ_{XY} is the angle between the V_{XY} and OS. D_{XOY} represents the distance between the SUR and the obstacle in the horizontal plane, and d_{xy} represents the shortest distance allowed between the SUR and the obstacle. U_{HD} and U_{Ht} are used to evaluate the shortest distance between the SUR and the obstacle and the time when the collision occurs, respectively.

Similarly, the vertical velocity potential U_V can be written as:

$$U_V = \begin{cases} U_{VD} \bullet U_{Vt} & if\,\theta_{xz} < \theta_V \\ 0 & else \end{cases} \tag{30}$$

where

$$\begin{aligned} \sin\theta_V &= \frac{d_{XZ}}{D_{XOZ}} \\ U_{VD} &= \frac{1}{D_{XOZ}} \bullet \left(\frac{1}{|\sin\theta_{XZ}|} - \frac{1}{\sin\theta_V}\right) \\ U_{Vt} &= \exp\left(-\frac{D_{XOZ}}{|V_{XZ}|\cos\theta_{XZ}}\right) \end{aligned} \tag{31}$$

If U_H and U_V are greater than 0, it means that the relative velocity vector V_{XY} and V_{XZ} are in the collision area. The larger the values of U_H *and* U_V, the higher the risk of SUR's collision. By adjusting the value of U_H *and* U_V, SUR makes a decision to avoid obstacles.

3.5. Multi-sensor optimal estimation

In practical applications, due to the different physical characteristics of each sensor, it is likely that there will be differences in accuracy between sensors. Therefore, in order to obtain more accurate results, the

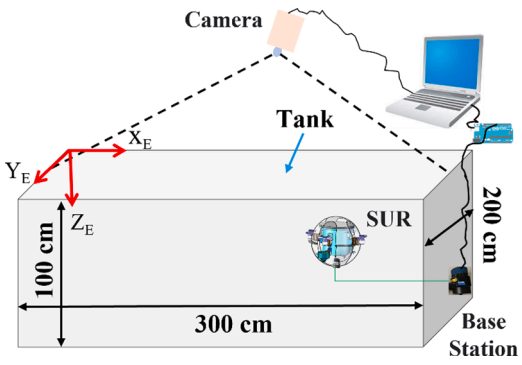

Fig. 9. Experimental platform for the SUR we setup.

data of each sensor is proportionally distributed during the processing. Assuming that the measurement is performed at time t, the measurement results of different sensors are:

$$\widehat{V}_{estimated} = W_{t_1} M_{t_1} + W_{t_2} M_{t_2} \tag{32}$$

where M_{t_1}, M_{t_2} represent the measured values of two independent sensors, and W_{t_1}, W_{t_2} indicate the weight of measured value of each sensor.

Then the estimated error can be described as:

$$F = E\left(\widetilde{V}_t^2\right) = (W_{t_1})^2 \delta_{t_1} + (I - W_{t_1})^2 \delta_{t_2} \tag{33}$$

Here, the cost function F is used to represent the root mean square error of $\widetilde{V}_{estimated}$ [45], as follows:

$$\widetilde{V}_{estimated} = V_{estimated} - \widehat{V}_{estimated} \tag{34}$$

where $\delta_{t_1}, \delta_{t_2}$ represent the random error, and W_{t_1}, W_{t_2} indicate the weight of measured value of each sensor.

To obtain the smallest cost function F, let $\varphi = (W_{t_1}, W_{t_2})$ and derivate φ.

$$\frac{\partial F}{\partial \varphi} = 0 \tag{35}$$

The optimized weight can be solved as:

$$W_{t_1} = \frac{\delta_{t_1}}{\delta_{t_1} + \delta_{t_2}}, W_{t_2} = \frac{\delta_{t_2}}{\delta_{t_1} + \delta_{t_2}} \tag{36}$$

According to Eq. (32), the best estimate simplifies:

$$\begin{aligned} \widehat{V}_{estimated} &= \frac{\delta_{t_1}}{\delta_{t_1} + \delta_{t_2}} M_{t_1} + \frac{\delta_{t_2}}{\delta_{t_1} + \delta_{t_2}} M_{t_2} \\ &= \frac{\delta_{t_1} \delta_{t_2}}{\delta_{t_1} + \delta_{t_2}} \left(\frac{1}{\delta_{t_1}} M_{t_1} + \frac{1}{\delta_{t_2}} M_{t_2} \right) \end{aligned} \tag{37}$$

The error covariance matrix after fusion is

$$\delta_t = \frac{\delta_{t_1} \delta_{t_2}}{\delta_{t_1} + \delta_{t_2}} \left(\frac{1}{\delta_{t_1}} + \frac{1}{\delta_{t_2}} \right)^{-1} \tag{38}$$

If there are N sensors, the measurement matrix are $\{M_{t_n}\}$, and $n = 1, 2, \cdots, N$ represents Gaussian white noise. Next, the weighting coefficients corresponding to the measured values of each sensor can be obtained based on the limit theory of multivariate function.

$$W_{t_q} = \frac{1/\delta_{t_n}}{\sum_{n=1}^{N} (1/\delta_{t_n})} \tag{39}$$

Thus, the error covariance matrix after fusion can be rewritten:

$$\delta_t = \left(\frac{1}{\delta_{t_1}} + \frac{1}{\delta_{t_2}} + \cdots + \frac{1}{\delta_{t_n}} \right)^{-1} \tag{40}$$

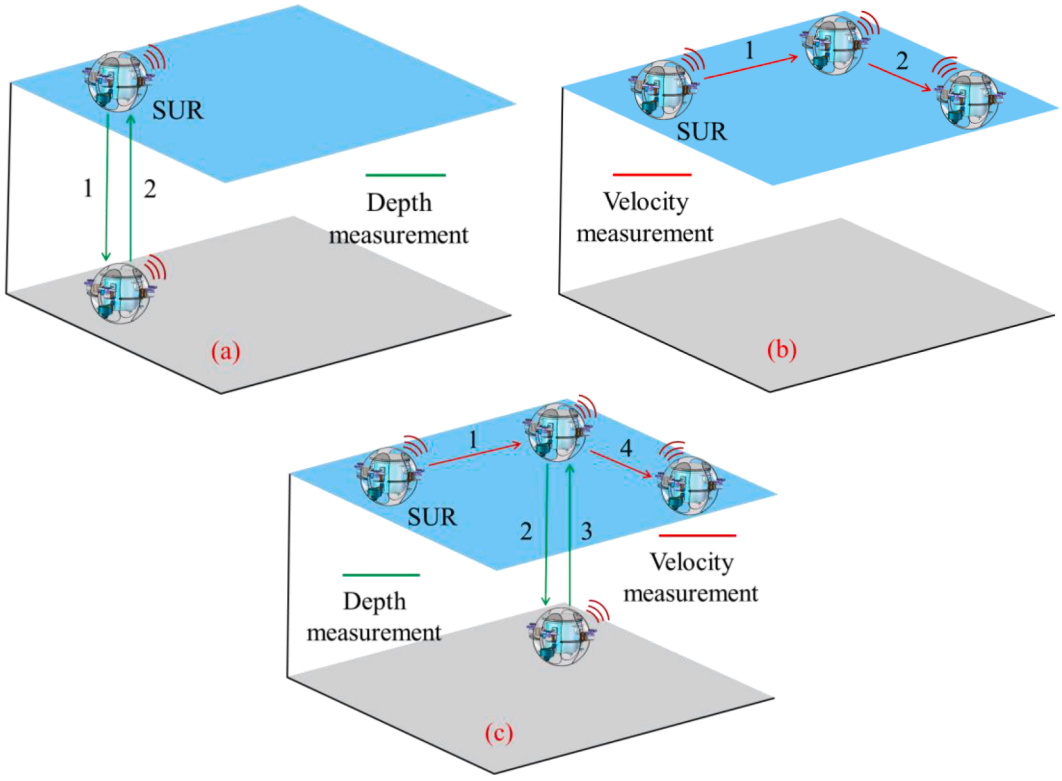

Fig. 10. Conditions used during underwater motion testing. (a) Diving and rising motion (b) Linear motion, The SUR started following the first linear track (1). Once the first endpoint was reached, it moved along the second linear track (2). (c) Comprehensive motion, the SUR started following the linear track (1). When the second endpoint was reached, it dived to the target depth. Once the third endpoint (3) was reached, at this time, the SUR rise to the surface. Next, the SUR followed the linear track (4) until reaching the target position.

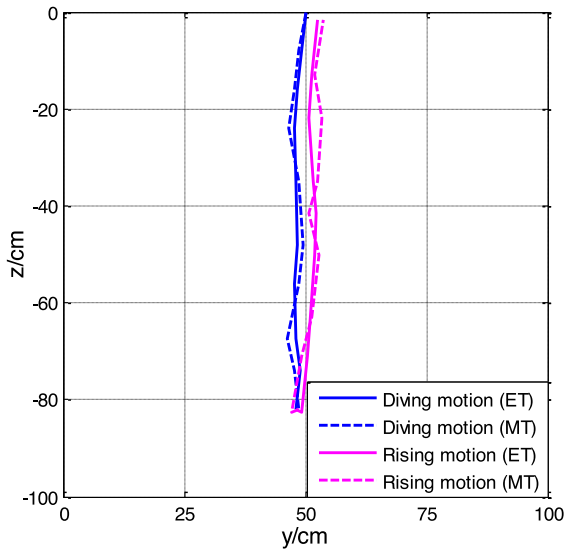

Fig. 11. Trajectory tracking result of the SUR in the diving and rising motion.

And the optimized estimate of MSIF model can be described as:

$$\widehat{V}_{estimated} = \delta_t \left(\frac{1}{\delta_{t_1}} M_{t_1} + \frac{1}{\delta_{t_2}} M_{t_2} + \cdots + \frac{1}{\delta_{t_n}} M_{t_n} \right) \tag{41}$$

4. Experimental results

In this section, we describe the experimental platform and perform some experiments, such as autonomous movement experiments, obstacle avoidance experiments, etc., to verify the performance of the proposed MSIF model.

4.1. Experimental description and setup

In this work, the MSIF model is used to achieve performance testing of SUR attitude estimation, positioning, and obstacle avoidance. Fig. 9 shows some experiments performed in a pool with the size of 300 cm x 200 cm x 100 cm (length x width x height). The water depth was about 80 cm. The observation system is mainly used to realize SUR two-dimensional position measurement and underwater data transmission. The attitude of the SUR is mainly monitored by the IMU and PSA. Specifically, the PSA data is pre-processed and trained by the motion state of SUR in still water, and the training method uses the BPNN machine learning tool.

To effectively verify the performance of the MSIF model, a series of experiments are performed. According to the motion characteristics of the SUR, see Fig. 8(a), a comprehensive evaluation of the performance of SUR is conducted. The specific metrics are as follows: pitch angle and roll angle, it is necessary to ensure that the pitch angle and roll angle swing around 0° in real time to adjust the attitude when performing tasks. Then, the data of DS and observation system are analysed to track the motion trajectory of SUR. Next, we evaluated the velocity and angle errors, etc., to verify the performance of the MSIF model. Finally, comparative experiments under different machine learning tools were conducted, which verified the accuracy, effectiveness and feasibility of BPNN and MSIF models.

4.2. Motion experiments and trajectories

Firstly, to validate the performance of the proposed MSIF model, three different conditions are set in the motion experiment, as shown in Fig. 10. Fig. S1 shows the tracking process of the SUR in motion experiments. Considering the dynamic nature of the experimental environment, it is not enough to conduct only a single experiment, so SUR repeats the experiment 5 times in each condition, and infers and trains the overall data by repeating the experiment multiple times.

Fig. 10(a) shows the diving and rising motions of the SUR. The SUR initially performs a diving motion until the target depth is reached, about 80 cm. After 1 s of stagnation, perform a rising motion to reorient back to the original starting position. The settings are as follows: the starting position is *(25 cm, 0 cm)*, and the target depth position is *(25 cm, −80 cm)*. The dataset only provides the part of the trajectory showing the target depth in *YOZ* plane, as shown in Fig. 11. Noted that the estimated trajectory and measured trajectory are represented by ET and MT, respectively. Then, we calculated the position error in the motion experiment, see Fig. 12. The total path length of the SUR is about 185 cm. The error between the two end points of the ET and MT is about 4.6 cm.

Fig. 10(b) shows the linear motion of SUR, the robot first moves along track (1), from starting position *(175 cm, 275 cm)*. After reaching the end point of track (1), continue to move along track (2) until reaching the target position *(25 cm, 25 cm)*. Fig. 13 shows the trajectory

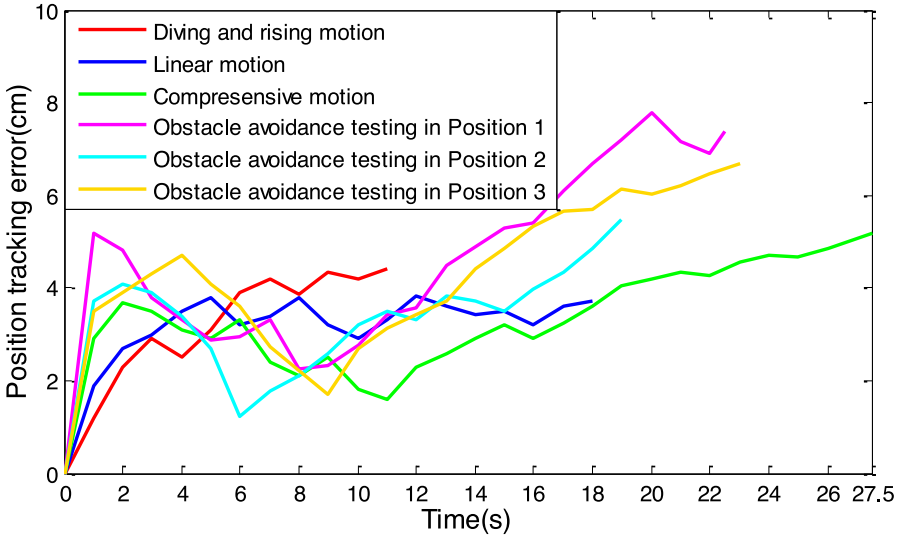

Fig. 12. Position tracking errors of the SUR in motion experiments and obstacle avoidance experiments.

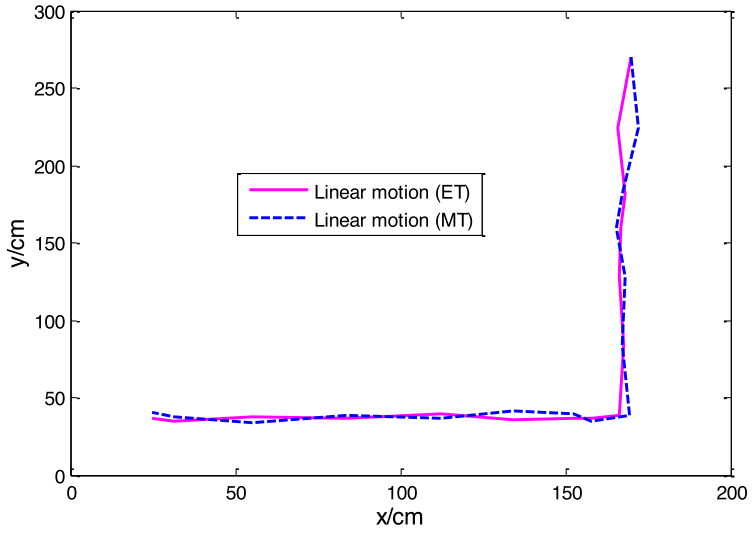

Fig. 13. Tracking result of the SUR in the linear motion.

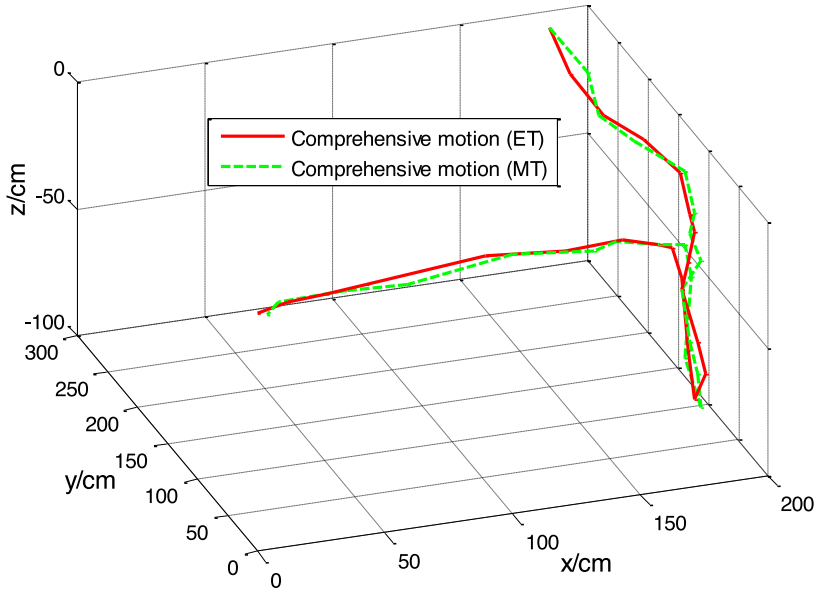

Fig. 14. Tracking result of the SUR in the comprehensive motion.

of the SUR in linear motion. The total time is 15 s. Besides, the position error, as shown in Fig. 12, between two end points is about 3.8 cm, while the total path is 452 cm.

In the comprehensive motion experiments, see Fig. 10(c), the SUR starts from the starting point *(175 cm, 275 cm, 0 cm)*, when the first endpoint is reached, the SUR dived to the target depth *(175 cm, 25 cm, −80 cm)*. Once the second endpoint is reached, the SUR stops and surfaces. When the target point *(25 cm, 25 cm, 0 cm)* is reached, the SUR stops moving. Fig. 14 shows the trajectory of the SUR in 18 s. Overall, in the comprehensive motion, the estimated trajectory reflects the change law of the measured trajectory well, the position error of the two end points, as shown in Fig. 12, is about 5.3 cm, and the total path length of the robot is about 635 cm.

4.3. Obstacle avoidance experiments and trajectories

Subsequently, to validate the performance of the MSIF model in the presence of obstacles, the obstacle avoidance experiment is tested from three different positions, as shown in Fig. 15. Fig. S2 shows the tracking process of the SUR in obstacle avoidance experiments. The settings are as follows: the SUR starts from three different positions, *Position 1 (25 cm, 25 cm), Position 2 (25 cm, 100 cm), Position 3 (25 cm, 175 cm)*, respectively, and cruises to the target position *(275 cm, 100 cm)*.

Fig. 16 shows the experimental result of the SUR in different positions. It can be seen that SUR can safely reach the target position after avoiding obstacles, and the trend of curves at different positions are approximately the same. Noted that around 10 s, there is a certain difference in the SUR's obstacle avoidance performance. Due to the position (see Fig. S2) of the *Obstacle 2* have a certain deviation under the action of the water waves. But the SUR can avoid obstacles successfully at the same time, and the error is less than 8 cm, as shown in Table 2. For each case and different positions, the obstacle avoidance performance further verifies the effectiveness and feasibility of the proposed MSIF model. Meanwhile, the experimental results of this study also offer an

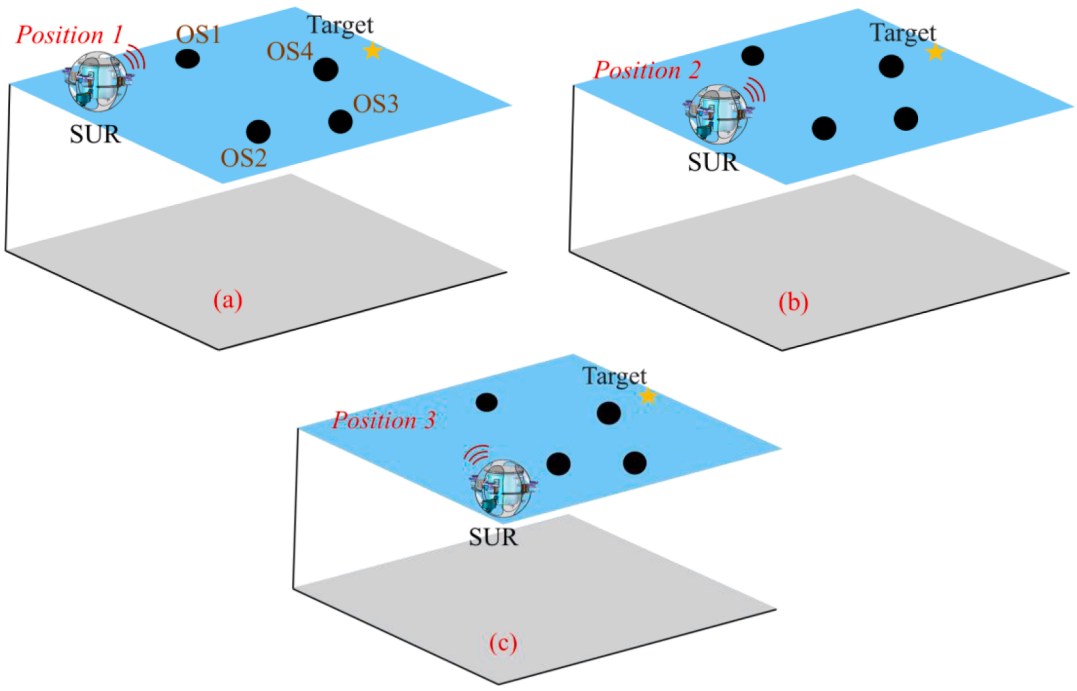

Fig. 15. Conditions used during underwater obstacle avoidance testing. (a) The SUR started moving from the *Position 1*. (b) Started at the *Position 2*. (c) Started at the *Position 3*.

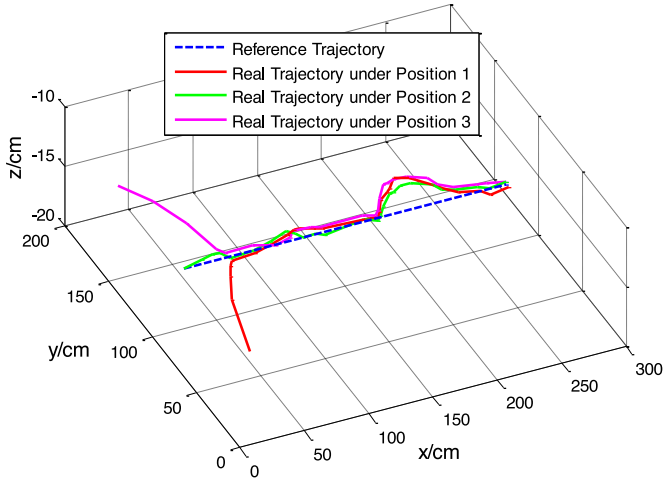

Fig. 16. Experimental results of SUR in different positions.

Table 2
Experimental results under different starting positions.

Case	Max position error [cm]	Min position error [cm]	Mean position error [cm]	Traveling time (s)
Position 1	7.89	2.26	5.18	22.5
Position 2	6.41	1.23	3.77	19
Position 3	7.56	1.72	4.59	23

intuitive and innovative design for the next generation of path planning strategies.

It can be known from Table 2 that when the starting position is different, the time spent by SUR is different. When the SUR starts from *Position 1* and *Position 3*, the required time is about 23 s, and the maximum position error is about 7.9 cm. The error difference between different positions is less than 2 cm. As shown in Fig. 12, the position error of the two end points in different positions is about 7.4 cm, 6.8 cm, 5.7 cm, respectively.

5. Discussion

After completing the above experiments, we further evaluate the comprehensive metrics to verify the performance of the MSIF model. Noted that the above experiments were all carried out under outdoor (Kagawa University, Takamatsu, Japan) conditions without further considering the practicability of the MSIF model for SUR in open waters such as rivers and lakes. In the future, we will further improve the related work. In addition, we also believe that the MSIF model is promising for autonomous motion and parameter estimation in scenarios such as lakes and rivers after evaluating the performance of the MSIF model.

In this section, we analyze the optimized parameters under various experiments to verify the MSIF model performance. A series of data is trained and validated using BPNN method. Experimental results show that the proposed MSIF model improves the accuracy of sensor measurements and reduces errors, compared to the data measured by a single type of sensor.

5.1. Experimental conditions analysis

In Fig. 12, we analyze the position error under different motion and obstacle avoidance experiments, the maximum position error is less than 8 cm. Next, we summarize the velocity and angle changes for different conditions to evaluate the performance of MSIF model. Fig. 17 shows the range of velocity, pitch and roll changes during and obstacle avoidance experiments.

From Fig. 17(a), it can be concluded that the velocity change in diving and rising motion is relatively stable during the movement. At about 5 s, the SUR reaches the end point of the track (1), see Fig. 10(a). Then perform the rising motion after about 1 s. At the same time, it can be seen that the MSIF effectively reduces the peaks caused by pitch and

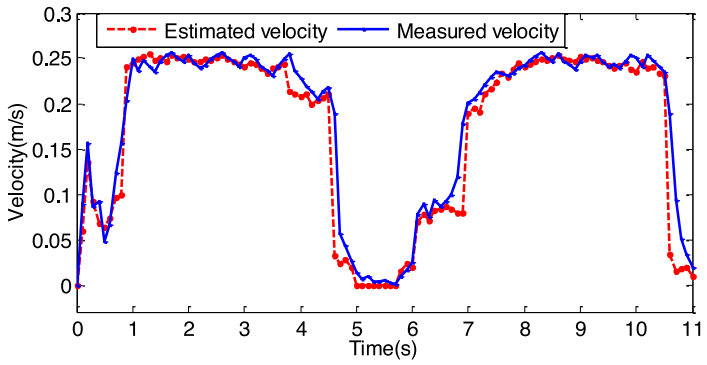

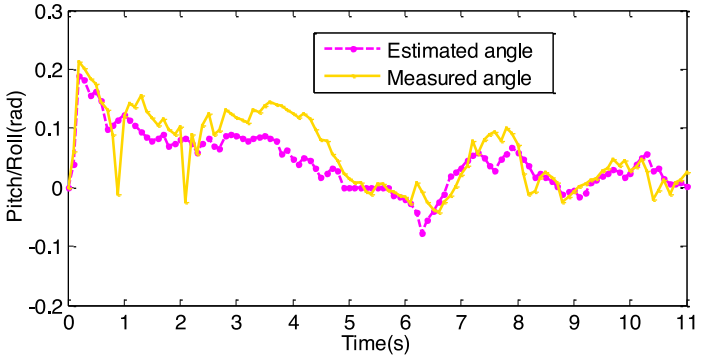

(a) velocity and angle change in diving and rising motion

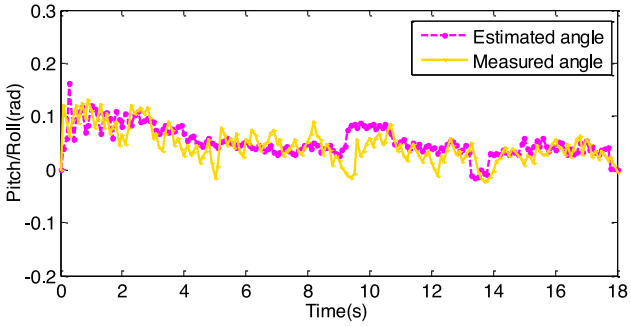

(b) velocity and angle change in linear motion

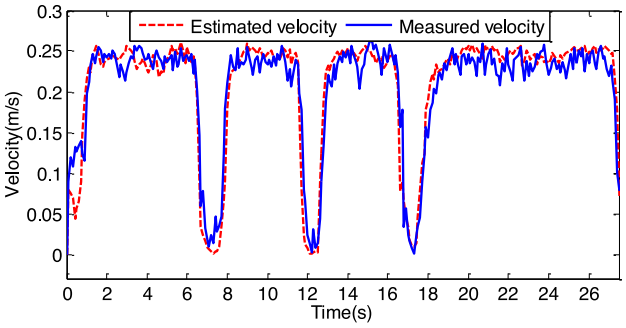

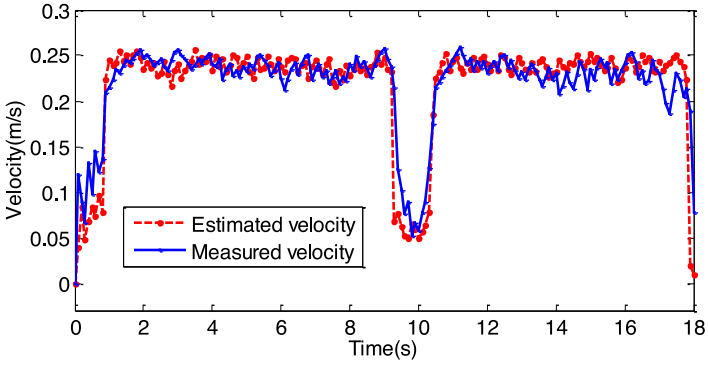

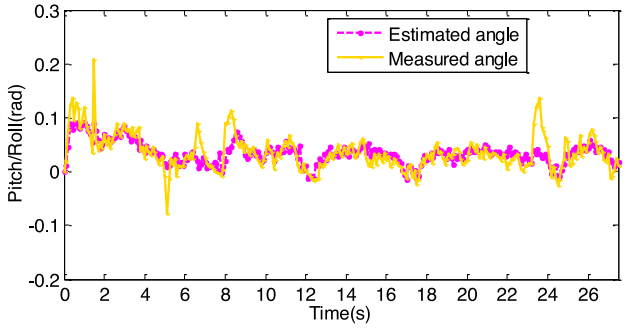

(c) velocity and angle change in comprehensive motion

Fig. 17. Estimated and measured velocity and angle of the SUR in motion experiments. (a) Estimated and measured velocity and angle in the diving and rising motion. (b) Estimated and measured velocity and angle in the linear motion (c) Estimated and measured velocity and angle in the comprehensive motion. (a) velocity and angle change in diving and rising motion (b) velocity and angle change in linear motion (c) velocity and angle change in comprehensive motion.

roll bias caused by the external environment (wave and surge motion, etc.), which may be particularly beneficial for the accuracy of SUR estimation and motion underwater in the future.

The incentive for linear motion is mainly to test the robustness of the SUR's velocity estimation during turns. Fig. 17(b) shows the velocity, pitch and roll angle changes of the SUR in linear motion, see Fig. 10(b). Especially during turning, about 7 s, the rapid drop in SUR velocity helps to track and control the steering safely. It can be seen that no significant deviation is observed during the turning. At the same time, it can be observed that the attitude angle can be adjusted in time during the movement and turning. The results further demonstrate that, together with the linear motion experimental results, the proposed MSIF model is able to perform reliable velocity and angle estimates for SUR common task trajectories, which further improves the expected accuracy and robustness.

The comprehensive motion includes linear motion, diving motion and rising motion, see Fig. 10(c). Fig. 17(c) shows the measured and estimated values of velocity and angle under combined motion within 27.5 s. The estimated velocity can track the measured velocity well, with an average absolute error of 0.0089 m/s and a maximum absolute error of 0.0652 m/s. Compared with the estimation results of robot velocity in [42,44], the MSIF model adopted in this paper can accurately estimate velocity and angle.

In the MSIF model, we incorporate the OASA, which improves the practicality of the model in natural conditions. For obstacle avoidance experiments (see Fig. 15), we verified the measured and estimated values of velocity and angle at different positions, as shown in Fig. 18. The percentage errors for each set of experiments were 5.43%, 3.89%, and 4.87%, respectively.

Considering all of the above, it can be concluded that the proposed MSIF model can accurately estimate the velocity and track the trajectory. The SUR's velocity and angle fluctuate widely at start and turn, then oscillate around a certain value, about 0.245 m/s. As we know, considering the combination of the estimated and measured linear velocities with less error. We fused and evaluated multiple sensors to establish reliable ground truth for velocity estimation and trajectory

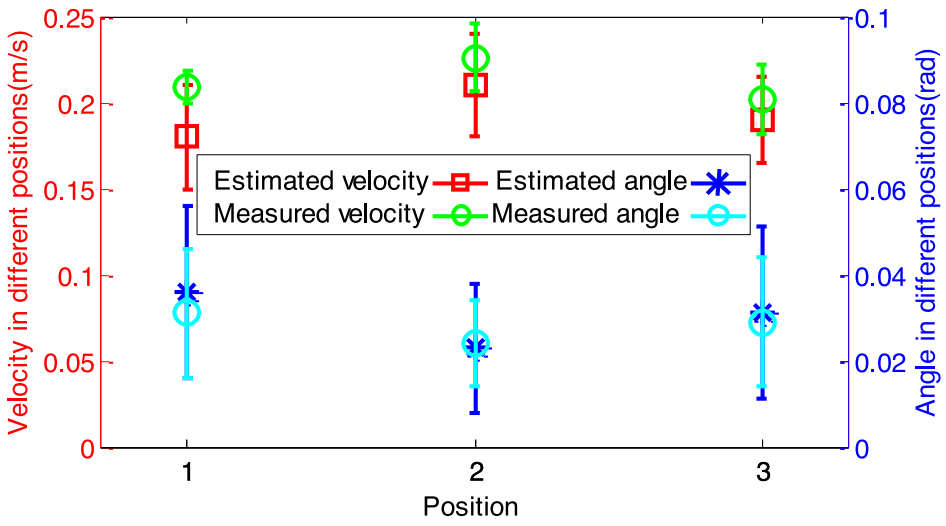

Fig. 18. Estimated and measured velocity and angle of the SUR in obstacle avoidance experiments (*Position 1, Position 2* and *Position 3*, see Fig. 15).

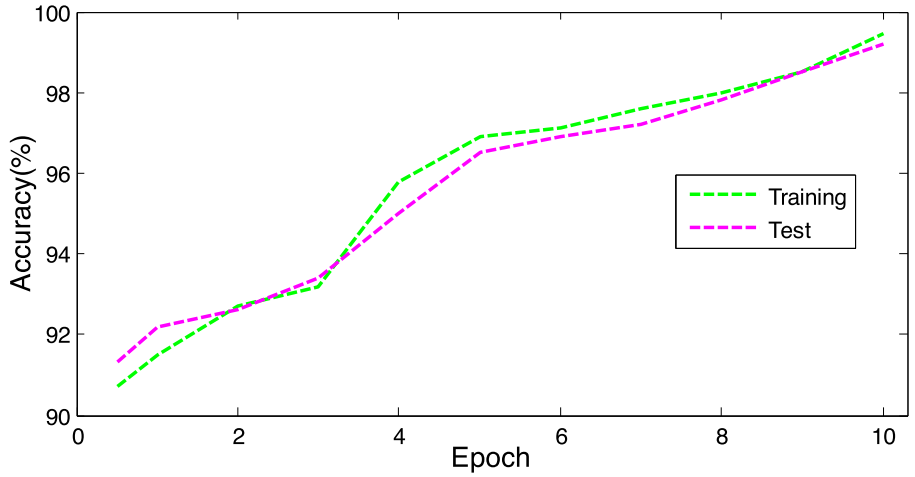

Fig. 19. Training and testing accuracy of the BPNN for 10 epochs.

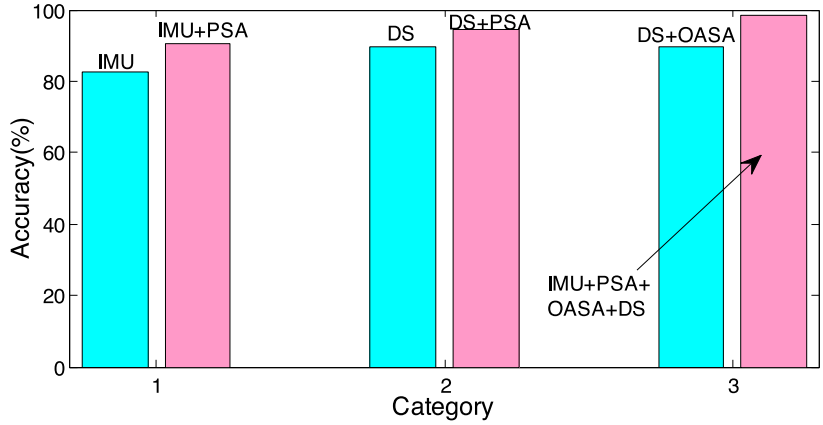

Fig. 20. MSIF model with BPNN analysis from the perspective of attitude (IMU and IMU+PSA), depth (DS and DS+PSA) and obstacle avoidance (DS+OASA and IMU+PSA+OASA+DS).

tracking. Therefore, this paper provides a promising approach for underwater robots using MSIF model.

5.2. Training and testing results based on BPNN

In Section 2.3, some machine learning tool methods are described and related parameters are set. Here, training results on multi-source

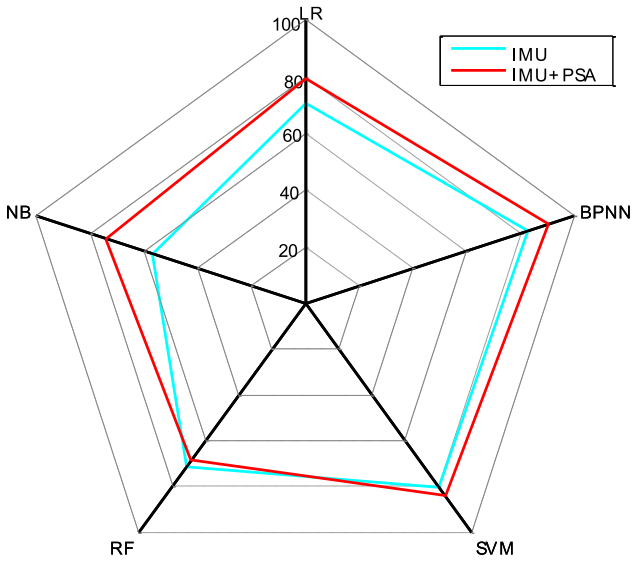

(a) IMU and IMU+PSA

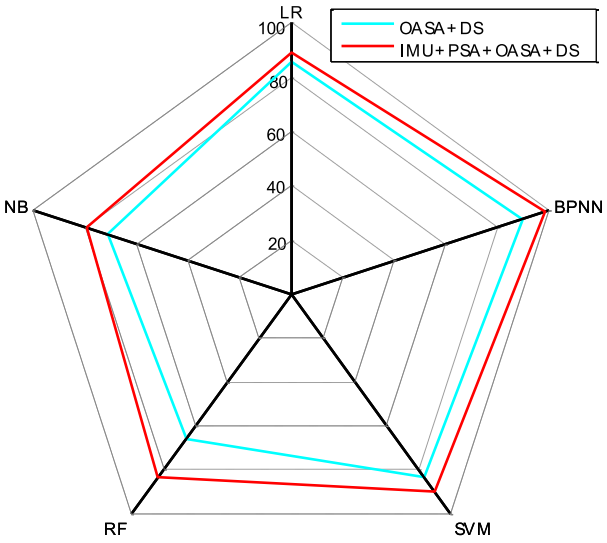

(c) DS+OASA and IMU+PSA+OASA+DS

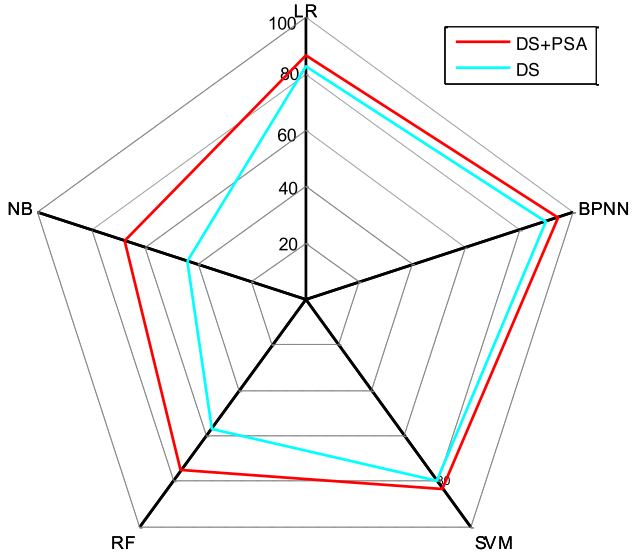

(b) DS and DS+PSA

Fig. 21. A comparison of the three categories using BPNN method with LR, NB, RF and SVM algorithms. (a) IMU and IMU+PSA (b) DS and DS+PSA (c) DS+OASA and IMU+PSA+OASA+DS.

information data are given.

Fig. 19 shows the accuracy plot of BPNN during training and testing for ten epochs. It can be seen that the training accuracy rate gradually increased, and finally converged at around 98.65%, while the test convergence was around 98.405%. Then, from the perspective of attitude, depth and obstacle avoidance, we divided the data types into three categories for analysis, namely IMU+PSA, DS+PSA, and IMU+PSA+OASA+DS. The training performance of the MSIF model with BPNN is validated by checking the accuracy of the three categories, as shown in Fig. 20. From the perspective of attitude adjustment, compared with the IMU self-resource, the average accuracy of the IMU+PSA is improved by 7.91%, which is about 90.55%. From the depth perspective, the average accuracy of DS+PSA is improved by 4.68% compared to self-resource DS, which is about 94.35%. From the perspective of obstacle avoidance, compared with OASA+DS, the average accuracy of IMU+PSA+OASA+DS based on the MSIF model is improved by 9.22%, about 98.65%. These results demonstrate that the proposed MSIF model can effectively improve the SUR's underwater attitude adjustment, positioning and obstacle avoidance skills.

Table 3
Comparison results of MSIF model under different machine learning tools.

Conditions	*NB (%)*	*RF (%)*	*SVM (%)*	*BPNN (%)*	*LR (%)*
IMU	56.78	71.25	80.52	82.64	70.53
IMU+PSA	73.97	68.56	84.21	90.55	79.46
DS	44.37	56.89	79.83	89.67	82.58
DS+ PSA	67.43	75.24	83.12	94.35	86.77
DS+OASA	71.34	65.87	83.59	89.43	85.71
IMU+PSA+DS+OASA	**79.53**	**83.46**	**90.26**	**98.65**	**89.32**

5.3. Comparison of the BPNN with other techniques

In this part, to further evaluate the performance of the MSIF model with BPNN method, we compared the BPNN method with Random Forest Algorithm (RF), Support Vector Machine (SVM), Naive Bayesian

Table 4
Performance comparison of RMSE for the proposed method and other studies.

Related efforts	Methods	Control mode	Prediction type	Results RMSE	Accuracy
Yang et al. [39], 2021	BPNN	Online	Regression	0.16	0.894
Li et al. [41], 2022	BPNN	Online	Regression	0.27	0.9825
Dong et al. [46], 2019	BPNN	Offline	Regression	0.353	0.774
Feng et al. [47], 2022	GA-BPNN-ARMA	Online	Classification	0.595	0.956
Liu et al. [48], 2020	BPNN	Online	Regression	0.0679	0.8405
This work	**BPNN**	**Offline/ Online**	**Regression**	**0.053/ 0.19**	**0.9865/ 0.981**

(NB), and Logistic Regression (LR). RF, SVM, NB and LR use the same preprocessed data from BPNN for training and testing. Fig. 21 shows the prediction accuracy under the five algorithms, it can be seen that the average test accuracy of IMU+PS+DS+OAS under NB, RF, SVM, LR and BPNN is 79.53%, 83.46%, 90.26%, 89.32% and 98.65, respectively. After the MSIF model using BPNN method, see Table 3, the maximum accuracy is improved by about 19.12%, compared to NB method. From the comparative outcome, the MSIF model with BPNN method contests well with the other classical methods (RF, SVM, NB and LR).

Furthermore, from the perspective of attitude with IMU and IMU+-PSA, the BPNN method is 11.39%, 2.12%, 25.86% and 12.11% more accurate than the RF, SVM, NB and LR algorithms, respectively. With IMU+PSA, outperforms 21.99%, 6.34%, 16.58% and 11.09%, respectively. In addition, from the perspective of DS, the BPNN method is 32.78%, 9.84%, 45.3% and 7.09% more accurate than the RF, SVM, NB and LR algorithms, respectively. With DS+PSA, outperforms 19.11%, 11.23%, 26.92% and 7.58%, respectively. By combining features extracted from multiple sensor datasets, it can be seen that the MSIF model achieves the best results using the BPNN method. These indicate that the MSIF model can help AUVs perform tasks safely and improve the performance efficiency of various skills in autonomous underwater motion.

In addition, we further analyzed the RMSE of this work, which is 0.053 and 0.19 offline and online, respectively. It is the smallest compared to a single type sensor node. Furthermore, we also compared with other studies, as shown in Table 4, it can be seen that the RMSE of this work is smaller than that of the methods proposed by *Yang* et al. [39], *Li* et al. [41], *Dong* et al. [46] and *Feng et al.* [47]. The accuracies are optimized by about 8.7%, 2.5% and 14.05%, respectively, compared to *Yang* et al. [39], *Feng et al.* [47] and *Liu* et al. [48]. Compared with the work of *Dong* et al. [46], the accuracy is optimized by about 21.25%. It is worth noting that in the previous work, most of the studies only focus on the training of a single control mode, this work considers both online or offline data training, which has more practical application value for AUVs.

As reflected by the experimental results, the proposed model exhibits very high accuracy in training using the BPNN method. In the context of machine learning, it is crucial to compare BPNN with other learning algorithms. It can be concluded that the BPNN method has similar accuracy to the SVM model when evaluating tool manipulation skills and experimental results in large datasets, which is also supported by [17,39, 49-50]. Notably, the adopted training model performs better than several other traditional machine learning models. This also proves that the combination of multi-source information is of great significance for the underwater movement and skill training of AUVs.

6. Conclusions

In this paper, we proposed a MSIF model for SUR to improve the practical application value in performing tasks. By constructing the optimized prediction models, such as attitude optimization model, velocity and depth estimation model, and obstacle avoidance model, the correlation and fusion scheme between multiple sensors in MSIF is developed. Then, the BPNN method was used for training and parameter optimization to improve the accuracy and effectiveness of the MSIF model. Next, a series of autonomous locomotion experiments and obstacle avoidance experiments were performed by integrating the MSIF model into our developed SUR to comprehensively evaluate performance metrics, including velocity, angle, and motion trajectory, etc. Some experimental results were drawn, as follows:

In the motion experiment, the SUR motion trajectory with an average absolute error is about 0.0089 m/s, and a maximum absolute error is about 0.0652 m/s. Compared with the obstacle avoidance experiment, the percentage errors for each set of experiments (*Position 1, Position 2* and *Position 3*) were 5.43%, 3.89%, and 4.87%, respectively. Further, the motion trajectory and attitude angle of the SUR are analyzed. The above experimental results prove that the MSIF model can accurately estimate the velocity and angle, and has greater advantages for SUR in attitude adjustment, positioning and obstacle avoidance. Subsequently, the accuracy of the adopted BPNN model was as high as 98.65%, which was 8.39%, 15.19%, 19.12% and 9.33% higher than that of SVM, RF, NB and LR, respectively. Then, the MSIF model was compared with other studies, the accuracy was optimized by about 8.7%, 2.5% and 14.05%, respectively, compared to *Yang* et al. [39], *Feng* et al. [47] and *Liu* et al. [48]; The RMSE was reduced by about 0.08, 0.3, 0.405, respectively, compared to *Li* et al. [41], *Dong* et al. [46], *Feng* et al. [47].

Based on the theoretical derivation and experimental results, it could be concluded that the proposed model offered high prediction accuracy for AUV's characteristic evaluation than individual data sources. The MSIF model proposed in this paper has a certain reference value for the fusion of other data sources, and also validates the importance of the MSIF model for optimizing the attitude, positioning and obstacle avoidance of AUVs.

CRediT authorship contribution statement

Chunying Li: Conceptualization, Methodology, Software, Writing – original draft, Funding acquisition, Investigation. **Shuxiang Guo:** Supervision, Writing – review & editing, Resources, Funding acquisition.

Declaration of Competing Interest

The authors declare that they have no known competing financial interests or personal relationships that could have appeared to influence the work reported in this paper.

Data availability

The data that has been used is confidential.

Acknowledgements

This work is supported in part by the Japan Society for the Promotion of Science (SPS) KAKENHI under Grant 15K2120, and in part by the China Scholarship Council (CSC) for his doctoral research at Kagawa University under Grant 202208050040.

Supplementary materials

Supplementary material associated with this article can be found, in the online version, at doi:10.1016/j.inffus.2023.02.024.

References

[1] C. Li, S. Guo, J. Guo, Tracking control in presence of obstacles and uncertainties for bioinspired spherical underwater robots, J. Bionic Eng. 20 (2023) 323–337.
[2] R. Liu, X. Cao, M. Liu, Y. Zhu, 6-DOF fixed-time adaptive tracking control for spacecraft formation flying with input quantization, Inf. Sci. (Ny) 475 (2019) 82–99.
[3] M. Kruusmaa, P. Fiorini, W. Megill, M. Vittorio, O. Akanyeti, F. Visentin, L. Chambers, H. Daou, M. Fiazza, J. Ježov, M. Listak, L. Rossi, T. Salumae, G. Toming, R. Venturelli, D. Jung, J. Brown, F. Rizzi, A. Qualtieri, J. Maud, A. Liszewski, FILOSE for Svenning: a flow sensing bioinspired robot, IEEE Robotics & Automation Magazine 21 (3) (2014) 51–62.
[4] C. Li, S. Guo, Adaptive multi-mode switching strategy for the spherical underwater robot with hybrid thruster, Adv. Eng. Inf. 55 (2023), 101845.
[5] C. Li, S. Guo, J. Guo, Study on obstacle avoidance strategy using multiple ultrasonic sensors for spherical underwater robots, IEEE Sens J 22 (24) (2022) 24458–24470.
[6] H.M. Xing, Y. Liu, S.X. Guo, L.W. Shi, X.H. Hou, W.Z. Liu, Y. Zhao, A multi-sensor fusion self-localization system of a miniature underwater robot in structured and GPS-denied environments, IEEE Sens. J. 21 (23) (2021) 27136–27146.
[7] H. Yin, S. Guo, M. Liu, A virtual linkage-based dual event-triggered formation control strategy for multiple amphibious spherical robots in constrained space with limited communication, IEEE Sens. J. 22 (13) (2022) 567–580.
[8] W. Luo, Study of attitude adjustment and positioning methods for navigational vehicles, J. Phys. Conference Series 1952 (3) (2021), 042043.
[9] R. An, S. Guo, Y. Yu, C. Li, T. Awa, Task planning and collaboration of jellyfish-inspired multiple spherical underwater robots, J. Bionic Eng. 19 (2022) 643–656.
[10] J. Wang, Z. Wu, H. Dong, M. Tan, J. Yu, Development and control of underwater gliding robots: a review, IEEE/CAA J. Automatica Sinica 9 (9) (2022) 1543–1560.
[11] T. Banerjee, S. Das, Multi-sensor data fusion using support vector machine for motor fault detection, Inf. Sci. (Ny) 217 (25) (2012) 96–107.
[12] Y. Wu, Y. Ma, S. Wan, Multi-scale relation reasoning for multi-modal visual question answering, Signal Process.: Image Commun. 96 (2021), 116319.
[13] F. Pau, M. Jose, G. Jorge, R. Anna, V. Mar, Multi-sensor data fusion calibration in IoT air pollution platforms, IEEE Internet of Things J. 7 (4) (2020) 3124–3132.
[14] C. Li, S. Guo, Performance evaluation of spherical underwater robot with attitude controller, Ocean Eng. 268 (2023), 113434.
[15] R. Yager, Set measure directed multi-source information fusion, IEEE Trans. Fuzzy Syst. 19 (6) (2011) 1031–1039.
[16] P. Zhang, T. Li, G. Wang, C. Luo, H. Chen, J. Zhang, D. Wang, Z. Yu, Multi-source information fusion based on rough set theory: a review, Inf. Fusion 68 (2021) 85–117.
[17] M. Liu, X. Yao, J. Zhang, W. Chen, X. Jing, K. Wang, Multi-sensor data fusion for remaining useful life prediction of machining tools by IABC-BPNN in dry milling operations, Sensors 20 (2020) 4657.
[18] X. Che, J. Mi, D Chen, Information fusion and numerical characterization of a multi-source information system, Knowl. Based Syst. 145 (1) (2018) 121–133.
[19] A. Weinstein, A. Cho, G. Loianno, V. Kumar, Visual inertial odometry swarm: an autonomous swarm of vision-based quadrotors, IEEE Robotics Automation Lett. 3 (3) (2018) 1801–1807.
[20] R. Mur-Artal, J.D. Tardós, ORB-SLAM2: an open-source slam system for monocular, stereo, and RGB-D cameras, IEEE Trans. Robotics 33 (5) (2017) 1255–1262.
[21] J. Zhang, S. Singh, Laser-visual-inertial odometry and mapping with high robustness and low drift, J. Field Robotics 35 (8) (2018) 1242–1264.
[22] T. Nguyen, M. Cao, S. Yuan, Y. Lyu, T. Nguyen, L. Xie, VIRAL-fusion: a visual-inertial-ranging-lidar sensor fusion approach, IEEE Trans. Robotics 38 (2) (2021) 958–977.
[23] R. Liu, K. Greve, P. Cui, N. Jiang, Collaborative positioning method via GPS/INS and RS/MO multi-source data fusion in multi-target navigation, Survey Rev. 54 (383) (2022) 95–105.
[24] H. Zhou, Y. Zhao, Q. Shen, L. Yang, H. Cai, Risk assessment and management via multi-source information fusion for undersea tunnel construction, Automation in Construction 111 (2020), 103050.
[25] J. Lighthill, Estimates of pressure differences across the head of a swimming clupeid fish, Philosophical Trans. Royal Soc. B 341 (1993) 129–140.
[26] P. Bao, L. Shi, Z. Chen, S. Guo, A vision-based underwater formation control system design and implementation on small underwater spherical robots, Machines 10 (10) (2022) 877.
[27] L. Shi, P. Bao, S. Guo, Z. Chen, Z. Zhang, Underwater formation system design and implement for small spherical robots, IEEE Syst. J. (2022) 1–11. Early Access.
[28] L. Shi, Y. Hu, S. Su, S. Guo, H. Xing, X. Hou, Y. Liu, Z. Chen, Z. Li, D. Xia, A fuzzy PID algorithm for a novel miniature spherical robots with three-dimensional underwater motion control, J. Bionic Eng. 17 (2020) 959–969.
[29] L. Shi, Z. Zhang, Z. Li, S. Guo, S. Pan, P. Bao, L. Duan, Design, implementation and control of an amphibious spherical robot, J. Bionic Eng. 19 (2022) 1736–1757.
[30] R. An, S. Guo, L. Zheng, H. Hirata, S. Gu, Uncertain moving obstacles avoiding method in 3d arbitrary path planning for a spherical underwater robot, Rob Auton Syst 151 (2022), 104011.
[31] S. Gu, S. Guo, L. Zheng, A highly stable and efficient spherical underwater robot with hybrid propulsion devices, Auton Robots 44 (2020) 759–771.
[32] C. Li, S. Guo, J. Guo, Performance evaluation of a hybrid thruster for spherical underwater robots, IEEE Trans. Instrumentation & Measurement 71 (2022) 1–10.
[33] R. An, S. Guo, Y. Yu, C. Li, T. Awa, Multiple bio-inspired father–son underwater robot for underwater target object acquisition and identification, Micromachines (Basel) 13 (1) (2022) 25.
[34] S. Gu, L. Zhang, S. Guo, L. Zheng, R. An, T. Jiang, A. Xiong, Communication and cooperation for spherical underwater robots by using acoustic transmission, IEEE/ASME Trans. Mechatronics (2022) 1–10.
[35] X. Hou, Z. Li, S. Guo, L. Shi, H. Xing, H. Yin, An improved backstepping controller with an LESO and TDs for robust underwater 3D trajectory tracking of a turtle-inspired amphibious spherical robot, Machines 10 (6) (2022) 450.
[36] B. Wei, Application of neural network based on multisource, Wireless Commun. Mobile Comp. 2022 (2022) 1–13.
[37] I. Afyouni, Z. Aghbari, R. Razack, Multi-feature, multi-modal, and multi-source social event detection: a comprehensive survey, Inf. Fusion 79 (2022) 279–308.
[38] A. Raja, S. Chukka, R. Jayaganthan, Prediction of fatigue crack growth behaviour in ultrafine grained Al 2014 alloy using machine learning, Metals (Basel) 10 (2020) 1349.
[39] Z. Yang, S. Guo, Y. Liu, H. Hirata, T. Tamiya, An intentionbased online bilateral training system for upper limb motor rehabilitation, Microsyst. Technol. 27 (1) (2021) 211–222.
[40] Y. Zhao, Wang Y. Zhang, J. Zhang, X. Liu, Y. Li, S. Guo, X. Yang, S. Hong, Surgical GAN: towards real-time path planning for passive flexible tools in endovascular surgeries, Neurocomputing 500 (21) (2022) 13395–13406.
[41] H. Li, S. Guo, H. Wang, D. Bu, Subject-independent continuous estimation of sEMG-based joint angles using both multisource domain adaptation and BP neural network, IEEE Trans. Instrumentation & Measurement 72 (2022), 4000910.
[42] M. Christian, F. Juan, P. Narcís, C. Marc, K. Maarja, Differential pressure sensor speedometer for autonomous underwater vehicle velocity estimation, IEEE J. Oceanic Eng. 45 (3) (2020) 946–978.
[43] M. Sharif, X. Tan, A pressure difference sensor inspired by fish canal lateral line, Bioinspir. Biomim. 14 (2019), 055003.
[44] Z. Zhang, C. Zhou, Z. Cao, M. Tan, L. Cheng, S. Deng, J. Fan, A speed measurement method for underwater robots using an artificial lateral line sensor, Smart Mater. Structures 31 (1) (2021), 015011.
[45] X. Zheng, W. Wang, M. Xiong, G. Xie, Online state estimation of a fin-actuated lateral line system, IEEE Trans. Robotics 36 (2) (2020) 472–487.
[46] Y. Dong, Y. Shao, X. Li, S. Li, L. Quan, W. Zhang, J. Du, Forecasting pavement performance with a feature fusion LSTM-BPNN model, in: Proceedings of the 28th ACM International Conference on Information and Knowledge Management, 2019, pp. 1953–1962. November 2019.
[47] H. Feng, M. Zhang, V. Gecevska, B. Chen, R. Saeed, X. Zhang, Modeling and evaluation of quality monitoring based on wireless sensor and blockchain technology for live fish waterless transportation, Comput. Electron. Agriculture 193 (2022), 106642.
[48] M. Liu, X. Yao, J. Zhang, W. Chen, X. Jing, K. Wang, Multi-sensor data fusion for remaining useful life prediction of machining tools by IABC-BPNN in dry milling operations, Sensors 20 (17) (2020) 4657.
[49] P. Ghamisi, B. Rasti, N. Yokoya, Q. Wang, B. Hofle, L. Bruzzone, F. Bovolo, M. Chi, K. Anders, R. Gloaguen, P. Atkinson, J. Benediktsson, Multisource and multitemporal data fusion in remote sensing: a comprehensive review of the state of the art, IEEE Geoscience and Remote Sensing Magazine 7 (1) (2019) 6–39.
[50] I. Nti, A. Adekoya, A. Weyori, A novel multi-source information-fusion predictive framework based on deep neural networks for accuracy enhancement in stock market prediction, J. Big Data 8 (17) (2021) 1–28.